# Vibration based structural health monitoring of a composite plate with stiffeners

**R. Loendersloot[1], T.H. Ooijevaar[2], L. Warnet[2], A. de Boer[1], R. Akkerman[2]**
[1] University of Twente, Faculty of Engineering Technology – Structural Dynamics and Acoustics,
P.O. Box 217, 7500AE Enschede, The Netherlands
e-mail: **r.loendersloot@ctw.utwente.nl**

[2] University of Twente, Faculty of Engineering Technology – Production Technology,
P.O. Box 217, 7500AE Enschede, The Netherlands

## Abstract
A vibration based damage identification algorithm is implemented to assess the damage of a thin–walled composite structure. The structure analysed is a skin with stiffeners, as frequently applied in aircraft components. Both experimental and numerical studies on a single composite skin–stiffener structure showed that the *modal strain energy damage index* (MSE–DI) algorithm is a suitable method for the detection and localization of a delamination of the stiffener from the skin. A recent study on a strip with a single stiffener and an artificial delamination is extended to a study on a plate with two stiffeners and an impact induced delamination damage.

## 1 Introduction

Development of structural health monitoring (SHM) technologies for composite based structural components for aircrafts is one of the objectives of the European research program Clean Sky / Eco–design. The skin–stiffener based structures, of which for example wing sections of an airplane are built, are of special interest. The connection between the skin and the stiffener is vulnerable for delamination damage. Hence, this section must be frequently tested or the part is replaced prior to its end of life, which is cost and resource inefficient.

Vibration based damage identification methods are promising as an alternative for the time consuming and costly non–destructive testing (NDT) methods currently available. The change of the dynamic properties is employed to identify damage such as delaminations. Damage detection based on a shift of the natural frequencies [1] allows for a detection, but localization of the damage is difficult, in particular if multiple damages are present. The *modal strain energy damage index* (MSE–DI) algorithm [2] is therefore adopted. This method is one of the vibration based damage identification methods currently available and is based on the observation that local changes in the model strain energy are a sensitive indicator of damage.

Experimental work is carried out to explore the capabilities of the MSE–DI algorithm in terms of detection and localization of a delamination. Subsequently, numerical models are employed to support the experimental observations and to enhance the prognostic capabilities of the algorithm. The latter is to be achieved by using the results of finite element models. These results provide insight in the expected change in the damage index due to damage in the form of a delamination.

Initially, measurements were performed on a composite strip with a single stiffener [3]. A numerical model was developed and validated on the experimental results [4, 5]. A parametric study was performed by varying the size and the location of the delamination as well as the number of data points used in the analysis. At that point, the numerical model was mainly used as a virtual experimental set–up, to prevent an extensive and

costly experimental program. Moreover, the capabilities of a numerical simulation of a delamination were explored. Currently, a number of developments is ongoing, continuing these first steps:

1. Implementation of a numerical model of a plate with multiple stiffener to be used to enhance the data interpretation of measurement data.
2. Measurements are performed on a composite plate with two stiffeners [6], which is to be extended to a relatively large plate with three or more stiffeners, representing a more realistic skin–stiffener structure as frequently applied in aircraft components.
3. An impact damage, of inherently unknown exact size and unstructured dimensions, is applied instead of creating a well–defined, artificial delamination during the production process.
4. A validation of the numerical model used, including non–linear effects at the location of the delamination.

The focus in this paper is on the development of the numerical models. In particular on the numerical model of the plate with multiple stiffeners. The experimental results of the plate under investigation are presented in [6]. The plate was subjected to an impact load, but this impact load was not included in the numerical model, as it would require damage models which are beyond the scope of this work.

The paper is structured as follows: First of all, a brief introduction on vibration based structural health monitoring (VB–SHM)is presented (section 2). The structure analysed is presented in section 3, followed by the theory of the MSE–DI algorithm in section 4, the implementation of the finite element model section 5. The results are discussed in section 6 and finally conclusions and a future outlook are presented in section 7.

## 2 Review on the modal strain energy damage index algorithm

The modal strain energy damage index algorithm is one of the many techniques available to assess the health of a structure in a non–destructive way. The position of the MSE–DI algorithm with respect to other non–destructive health monitoring techniques is presented in the non–exhaustive overview in figure 1. The MSE–DI algorithm is a member of the family of vibration based structural health monitoring technologies (VB–SHM). VB–SHM can offer some specific advantages compared to other NDT technologies, in particular regarding the ability to assess the health of the structure online, i.e. during operation of the structure.

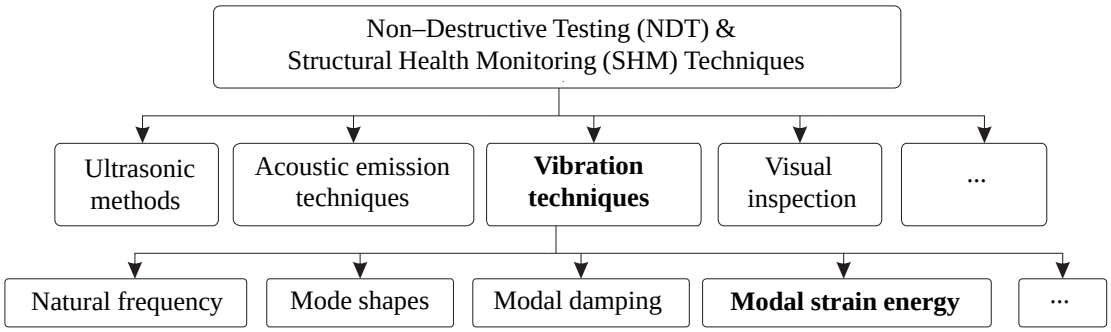


Figure 1: *Position of the Vibration Based Structural Health Monitoring techniques with respect to other damage identification methods.*

In the early 90s, Stubbs et al. [2, 7] presented the modal strain energy damage index (MSE–DI) algorithm and applied it to a steel bridge. The core of the MSE–DI algorithm consist of the phenomenon that the modal strain energy of a vibrating structure exhibits local discontinuities due to a loss in stiffness. The modal strain

energy is determined from a modal analysis. In general, only a limited number of natural mode shapes is required to determine the damage index and it does not rely on a normalisation of the modes shapes [8, 9]. The magnitude of the damage index is used to estimate the severity of the damage [10].

Farrar and Jauregui [8, 9] compared the MSE–DI algorithm to methods based on the mode shape curvature [11], flexibility coefficients [12], stiffness coefficients [13] and the curvature of the uniform load surface [14]. They used both experimental data and a numerical model of the steel bridge discussed in [2]. Their final conclusion is that the MSE–DI algorithm is the most powerful method. Alvandi and Cremona [15] also assessed different vibration based damage identification techniques. They focussed on the performance of different methods considering experimental data including a certain level of noise. Strain energy based methods are concluded to be the most stable methods.

The 1D MSE–DI algorithm is applied to 3D off–shore frame structures by Li et al. [16, 17]. Failure is assessed at truss level. The results are promising, but the stiffness reductions relatively large (5% stiffness reduction for a complete truss element) compared to the stiffness reductions caused by delaminations as discussed here. The main advantage is that the structural safety can be monitored during operation despite the difficult accessibility of the structure or visibility of the damage. This advantage also applies for (skin–stiffener) composite components, which are subject of this research, or for composite sandwich structures, as studied by Kumar et al. [18].

Here, the 1D algorithm is applied to a plate structure with two perpendicularly positioned strips. This so–called skin–stiffener construction is frequently applied in aerospace application to increase the stiffness without a severe weight penalty. It could be argued to implement 2D– or 3D–dimensional theory. However, it was shown by [6, 19] that the extension from 1D– to 2D–dimensional theory for the analysis of plates does not increase the sensitivity of the MSE–DI algorithm to detect and localize damage. Choi et al. [20, 21] and Kim et al. [22] concluded from their research to damage identification on plate structures that a compliance based damage index outperforms the strain energy based damage index algorithm, but they do not provide a comparison with a 1D approach.

The MSE–DI algorithm relies for practical applications on dynamic measurements. Inevitably, these dynamic measurements suffer from noise resulting in a probability of false damage identifications. Statistical methods are therefore employed to assess the performance of the damage detection method [15]. The dynamic response is often measured in the time domain [3, 23]. Subsequently, the data transformed to the frequency domain in which the modal parameters are determined. This method always requires an excitation, either as impact or (chirp) frequency sweep [3]. Alternatively, the time signal of vibrations occurring during operation can directly be used to determine the mean strain energy, by averaging over a fixed time interval. Choi and Stubbs [24] and Kim et al. [25] showed that this method can used to calculate the strain energy damage index and detect and localize damage equally well compared to the modal strain energy damage index.

## 3 Composite skin with stiffener structures

The structure investigated here is a composite skin–stiffener section. This type of stiffening is frequently used in aerospace components to increase the bending stiffness of the component without a severe weight penalty. Recently, a new type of skin–stiffener connection, depicted in figure 2, was developed by Fokker Aerostructures, in collaboration with the Dutch National Aerospace Laboratories (NLR). A PEKK (PolyEtherKatoneKatone) injection moulded filler is used as a connection. The fabrication process for this type of stiffener is presented in [26]. This type of stiffener connection is referred to as a T–joint.

The structure analysed in this paper is shown in figure 3. This skin–stiffener structure with the dimensions as indicated in the figure, is also subjected to dynamic measurements [6]. The composite is built from 16 individual plies of uni–directional co–consolidated carbon AS4D reinforced PEKK. A $[45/90/-45/0/45/90/-45/0]_s$ lay–up was used. Details on the experimental method used can be found in [3].

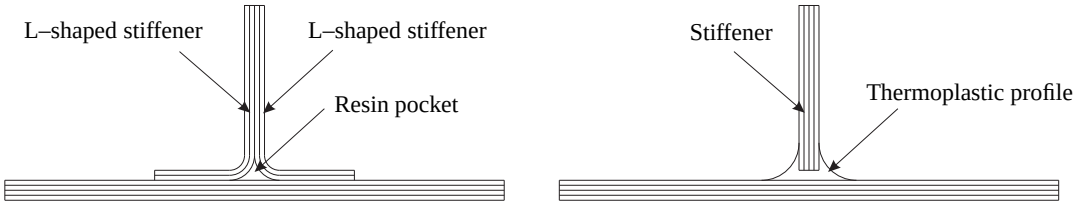


(a) *Traditional stiffener* (b) *New stiffener concept*

Figure 2: *Traditional double L–shaped stiffener versus the new stiffener concept developed by Stork–Fokker AESP and the NLR*

A typical damage occurring to composite structures is delamination. The location with the highest risk of failure of the structure is the region around the injection moulded thermoplastic T–joint profile which connects the stiffener to the skin. This was also observed in the impact experiments performed. A local impact was applied with the help of a DYNATUP 8250 falling weight impact machine. A repeated impact up to 10J resulted in significant but barely visible damage (BVID). Visual inspection showed that the damage at least consists of first ply failure and interface failure between the skin and the T–joint profile. The damaged region is indicated in figure 3. More details on the measurements can be found in [6].

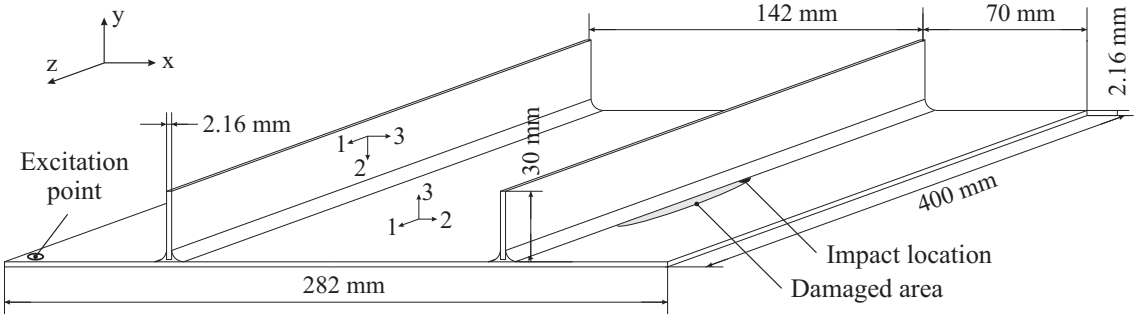


Figure 3: *The stiffened panel analysed. It has a [45/90/-45/0/45/90/-45/0]* $_s$ *laminate lay–up. The global coordinate system is indicated by* $xyz$*, whereas the local material coordinate systems of the skin and stiffeners are indicated by 123.*

## 4 Theory of the modal strain energy damage index algorithm

The strain energy of a vibration mode is referred to as the modal strain energy of that mode. Consequently, the total modal strain energy is the sum of the modal strain energy contributions of all modes considered. The modal strain energy is calculated by linking the deformation of a structure to the strain. A distinction must be made between axial, flexural and torsional deformation–strain relations. Only the bending strains are analysed, since bending is the main deformation in the structure and found to be the most sensitive to damage [4, 5]. Note that this does not imply that only (pure) bending modes are used in the analysis, since torsion modes also contain bending. As mentioned in section 2, a 1D formulation of the MSE–DI algorithm is implemented. Hence, only 1D theory is presented here. The mechanical relations read

$$\frac{\partial^2 u_y}{\partial x^2} = \frac{M_z}{EI_z}, \quad \frac{\partial^2 u_y}{\partial z^2} = \frac{M_x}{EI_x}, \tag{1}$$

with $u$ the displacement, $M$ the bending moment and $EI$ the bending rigidity of the structure. The cartesian global coordinate system $xyz$ is defined in figure 3 (the local material coordinate systems are indicated by 123). The bending related strains in two directions ($x$ and $z$) are used. The remainder of the derivation of the damage index is based on the bending terms in $z$–directions. Replacing $x$ by $z$ and vice versa gives the

relations to for the bending in $x$ direction. The strain energy (1D formulation) is found by integrating the squared strains over the length $l$ of the structure [27]

$$U = \frac{1}{2}\int_0^l EI_x \left(\frac{\partial^2 u_y}{\partial z^2}\right)^2 \mathrm{d}z. \tag{2}$$

Consider the structure to be vibrating in the $n^{\text{th}}$ mode. The displacement amplitude for the mode shape is $u_y^{(n)}(z)$. As a result, the modal strain energy of the $n^{\text{th}}$ mode is written as

$$U^{(n)} = \frac{1}{2}\int_0^l EI_x \left(\frac{\partial^2 u_y^{(n)}(z)}{\partial z^2}\right)^2 \mathrm{d}z. \tag{3}$$

Subsequently, the structure is discretised in $N$ elements in axial ($z$) direction. The strain energy $U_i^{(n)}$, due to the $n^{\text{th}}$ mode and associated with the $i^{\text{th}}$ element is then given by

$$U_i^{(n)} = \frac{1}{2}\int_{z_{i-1}}^{z_i} (EI_x)_i \left(\frac{\partial^2 u_y^{(n)}(z)}{\partial z^2}\right)^2 \mathrm{d}z \quad \text{with:} \quad U^{(n)} = \sum_{i=1}^{N} U_i^{(n)}. \tag{4}$$

Similar quantities can be defined for a damaged structure, using the mode shapes $\tilde{u}^{(n)}$ of the damaged structure. The local fractional strain energies, as defined by Cornwell et al. [19], are

$$F_i^{(n)} = \frac{U_i^{(n)}}{U^{(n)}} \quad , \quad \tilde{F}_i^{(n)} = \frac{\tilde{U}_i^{(n)}}{\tilde{U}^{(n)}}, \tag{5}$$

for the intact and damaged structure respectively. The fractional strain energy remains relatively constant in the intact elements, under the assumption that the damage is primarily located at a single element $\left(F_i^{(n)} = \tilde{F}_i^{(n)}\right)$ and that the rigidity does not change over an element [15, 19]. It can then be derived for element $j$ that

$$(EI_x)_j \int_{z_{j-1}}^{z_j} \left(\frac{\partial^2 u_y^{(n)}(z)}{\partial z^2}\right)^2 \mathrm{d}z \Big/ U^{(n)} = (\widetilde{EI}_x)_j \int_{z_{j-1}}^{z_j} \left(\frac{\partial^2 \tilde{u}_y^{(n)}(z)}{\partial z^2}\right)^2 \mathrm{d}z \Big/ \tilde{U}^{(n)}. \tag{6}$$

These equations are rearranged to obtain the quotient of the flexural rigidities, assuming the change of the total stiffness is negligible [15, 19],

$$\frac{(EI_x)_j}{(\widetilde{EI}_x)_j} \equiv \frac{\tilde{f}_j^{(n)}}{f_j^{(n)}} \tag{7}$$

with $f_j$ and $\tilde{f}_j$ equal to the integrals

$$f_j = \int_{z_{j-1}}^{z_j} \left(\frac{\partial^2 u_y^{(n)}(z)}{\partial z^2}\right)^2 \mathrm{d}z \Big/ \int_0^l \left(\frac{\partial^2 u_y^{(n)}(z)}{\partial z^2}\right)^2 \mathrm{d}z \quad , \tag{8}$$

$$\tilde{f}_j = \int_{z_{j-1}}^{z_j} \left(\frac{\partial^2 \tilde{u}_y^{(n)}(z)}{\partial z^2}\right)^2 \mathrm{d}z. \Big/ \int_0^l \left(\frac{\partial^2 \tilde{u}_y^{(n)}(z)}{\partial z^2}\right)^2 \mathrm{d}z \tag{9}$$

The local damage index $\beta$ for the $j^{\text{th}}$ element can be obtained by using the definition proposed by Stubbs et al. [2], which is a summation of the fractions $f_j^{(n)}$ over the number of modes considered

$$\beta_j = \sum_{n=1}^{N_{\text{freq}}} \tilde{f}_j^{(n)} \Big/ \sum_{n=1}^{N_{\text{freq}}} f_j^{(n)} \tag{10}$$

Note that this implies that not all modes need to be included. Including a large number of modes is expected to increase the sensitivity, since there more likely that at least one mode is affected. However, including a large number of modes also implies the magnitude of the effect is averaged over more modes and hence results in a lower damage index. As a result, it can be advantageously to discard a number of modes.

# 5 Finite Element Model

The numerical model is based on a finite element (FE) model. The objective was to develop a comparatively simple model with low computational requirements, allowing a large number of cases to be evaluated. Hence, a balance must be established between accuracy of the solution and complexity of the model. A shell element formulation is adopted since the plate and stiffener are both thin–walled. Experimental results [3] were used for a basic validation and to assess the validity of the approximations made in the model. The shell element based FE–model of the strip with single stiffener [4, 5] proved to predict the natural frequencies of the both the intact and damage structure accurately. Hence, the same approach is adopted to model the plate with multiple stiffeners. The PEKK injection moulded filler for the T–joint is not incorporated in the model.

Both the skin and the stiffeners consist of 16, quasi–isotropic stacked layers of fabric. The structure analysed here, is built from uni–directional layers allowing the use of the classical laminate theory (CLT) [28] to calculate the homogenised material properties of the composite laminate straightforwardly. The composite laminates are modelled using a double layer of shells, with reduced integration and three integration points over the thickness (ABAQUS© element type S4R, Simpson's rule for shell section integration). An orthotropic material definition is used. The material data, provided by Fokker Aerostructures, is obtained from static tests performed with samples of the batch used for the manufacturing of the T–beam that was measured [3]. The resulting homogenised material data used in the model is listed in table 1.

Table 1: *Homogenised material properties of the uni–directional composite, based on the measured material data.*

| $E_1 = E_2$ | $E_3$ | $\nu_{12} = \nu_{13}$ | $\nu_{23}$ | $G_{12} = G_{13} = G_{23}$ | $\rho$ |
|---|---|---|---|---|---|
| 72GPa | 10.5GPa | 0.30 | 0.45 | 5.56GPa | 1590kg·m$^{-3}$ |

Modelling a delamination generally involves non–linearities, due to the opening and closing of the delamination during cyclic deformation of the structure and friction between the two faces of the delamination[1]. This requires explicit solvers and time–domain simulations. Small time–steps must be used, given the frequency range of interest (up to 2000Hz), as is also indicated by Ullah and Sinha [29]. Alternatively, a 'free mode' model [30] can be used, which sets an upper bound for the effect of a delamination on the dynamic response of the structure: The nodes are doubled at the location of the delamination, hence share the same location, but there is no interaction defined between the surfaces of the delamination. Consequently, the elements on either side of the delamination can penetrate each other, effectively causing a lower stiffness and absence of damping induced by contact during cyclic closing of the delamination. On the other hand, it allows linear theory to be applied and simulations can be performed in the frequency domain, employing a linear perturbation based analysis. This saves a considerable amount of computation time. Evidently, the validity of this assumption must be checked by a comparison with experimental results or alternatively a numerical simulation in the time domain.

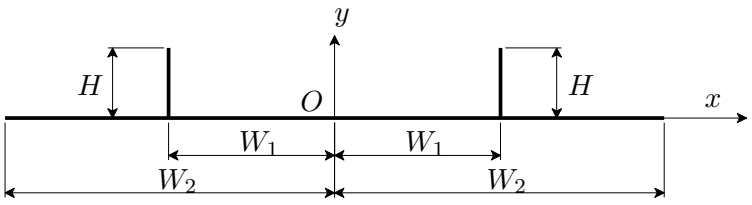


Figure 4: *Cross–section of the skin–stiffener structure.*

The delamination induced by the impact loading was observed to be located in the first layers below the

[1]Damage propagation is not accounted for, as the time scale of damage propagation must be significantly smaller than the time scale of the vibration. If not, the damage detection will coincide with actual failure of the structure.

surface at which the stiffeners are placed, as previously mentioned. Moreover, the impact was applied directly underneath the stiffener, as this was found to be the location with the highest risk of failure during impact experiments by Fokker Aerostructures.

The dimensions of the skin–stiffener model are presented in figure 4 and listed in table 2. A parametric FE–model is implemented, based on an extrusion of the cross–section in the $xy$–plane. The origin $O$ is positioned in the middle of the skin cross–section. Consequently, the stiffeners are positioned at $x = \pm W_1$ and the skin extents to $x = \pm W_2$. The top of the stiffeners is defined in $(x, y) = (\pm W_1, H)$. Subsequently, the cross–section is extruded in $z$–direction over a distances of $L$. The number of elements is set in different sections, resulting in a structured grid of nodes and elements with an aspect ratio close to 1. The number of elements in each section is also given in table 2.

Table 2: *Dimensions and number of elements in the different sections of the skin–stiffener structure.*

| Dimension | [mm] | Section | | | # Elements | Edge Length [mm] |
|---|---|---|---|---|---|---|
| $W_1$ | 71 | 0 | to | $W_1$ | 14 | 5.07 |
| $W_2$ | 70 | $W_1$ | to | $W_2$ | 14 | 5 |
| $H$ | 30 | 0 | to | $H$ | 8 | 3.75 |
| $L$ | 400 | 0 | to | $L$ | 80 | 5 |

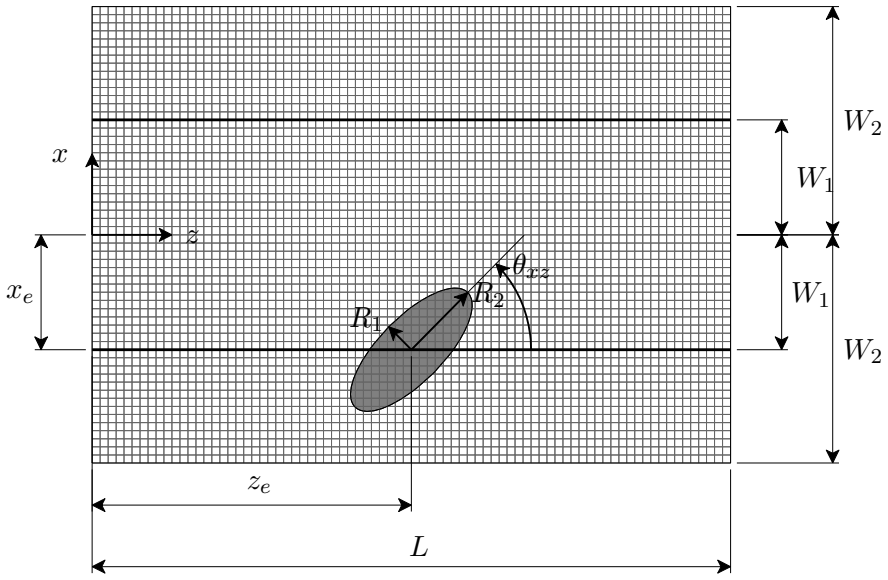


Figure 5: *Top view of the skin–stiffener plate ($xz$–plane). The gray area indicates the delamination. Nodes in this area are split, allowing the elements from top and bottom to deform independently from each other.*

A top view of the plate ($xz$–plane) is shown in figure 5. The delamination is defined as an ellipse (gray area in figure 5), with radii $R_1$ and $R_2$, with a central location defined in $\boldsymbol{x}_e = (x_e, 0, z_e)$ and an orientation angle $\theta_{xz}$ with respect to the $z$–axis. The nodes that are split obey the inequality relation

$$\left(\frac{x'_e - x'_i}{R_1}\right)^2 + \left(\frac{z'_e - z'_i}{R_2}\right)^2 < 1, \tag{11}$$

with the apostrophe indicating the coordinates in the local, rotated coordinate system (with respect to the global coordinate system $xyz$), according to

$$\begin{aligned} x' &= \phantom{-}x\cos\theta + z\sin\theta, \\ z' &= -x\sin\theta + z\cos\theta. \end{aligned} \tag{12}$$

A frequency analysis is performed using ABAQUS©. The structure is fully unconstrained, hence six rigid body modes will also be found by the solver. These are discarded.

# 6 Results & discussion

A number of geometrical parameters in the model was changed in order to assess the capabilities of the MSE–DI algorithm to detect and localize a delamination. The two radii of the ellipse representing the delamination are varied independently, the centre of the delamination is varied and the angle of the ellipse is varied. The variations, comprising a total of 18 different cases, are listed in table 3. The results are compared to the experimental results, attempting to find the most likely damage scenario (size, location and orientation of the delamination after the impact load). Note that the exact dimensions of the damage are unknown.

Table 3: *Variations applied in the geometry of the delamination.*

| Variable | Range | Unit | Total |
|---|---|---|---|
| $R_1$ | [0.01,0.015,0.02] | m | 3 |
| $R_2$ | [0.025,0.035,0.045] | m | 3 |
| $x_e$ | -0.071 | m | 1 |
| $z_e$ | 0.02 | m | 1 |
| $\theta$ | [0,-45] | $^{\circ}$ | 2 |
| total number | | | 18 |

The numerically calculated nodal displacements $u$ of the skin in all three cartesian directions are collected for each natural mode (the velocities were measured [3, 6]). The general procedure to calculate the damage index from the nodal displacements of the natural modes is presented in figure 6 for both the numerical model and the experiments. In the FE model, the nodal spacing along both the $x$– and $z$–direction is constant and nearly equal (aspect ratio of approximately 1). Therefore it is not needed to re–map the nodal displacements. The reason to use an equidistant grid is that a locally higher nodal density should not affect the results. Cubic splines are fit through the nodal displacements to obtain the mode shape functions. The standard spline function available in MATLAB© is employed. The spline is evaluated at 129 points (the total number of elements $N$ in (4) equals 128). The spline fit settings must be set with care to avoid numerical noise. This applies in particular for the measured data, which inherently contain measurement noise.

## 6.1 Comparison between the numerical model and the experiments

A basic validation of the numerical model was performed for the slender beam with single stiffener [4, 5]. The natural frequencies were predicted well, with a averaged relative error of 1.3% (maximum 5.5%) for the bending modes. Torsion modes showed a larger deviation (4.1% averaged, 7.6% maximum) with respect to the measurement. The mode shapes were also predicted well, indicating that the model was viable to be used.

However, the deviations in the natural frequencies and mode shape of the numerical model and the measurements of the skin with two stiffeners are significantly higher compared to the deviations found in for the beam with single stiffener. The natural frequencies up to 2000Hz of the numerical model are listed in table 4 and compared with the frequency of the matching mode shape of the measurements (between brackets the number of the experimental mode). Not all numerical modes could be matched with an experimental mode. The discrepancies are attributed to a number of reasons.

Firstly, the structure was suspended using rubber strings during the measurements and a force excitation. As a consequence, the assumption that the structure is fully unconstrained is not entirely correct. Both the

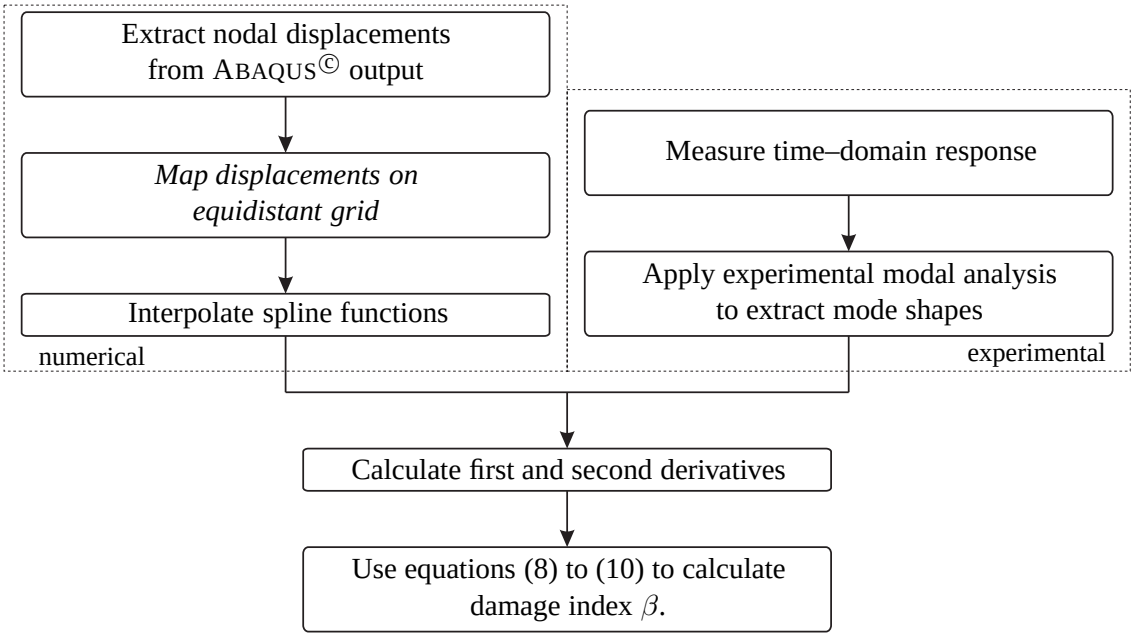


Figure 6: *General procedure to calculate the modal strain energy damage index, for numerical and experimental analysis. The second step of the numerical procedure is only required if a non-equidistant grid is used.*

Table 4: *Comparison of the numerical and experimental natural frequencies in Hz ($f_{N,num}$ and $f_{N,exp}$ respectively) up to 2000Hz. Not all numerical modes could be linked to an experimental mode. The sequence number of the experimental mode is given between brackets.*

| nr. | $f_{N,num}$ | $f_{N,exp}$ | nr. | $f_{N,num}$ | $f_{N,exp}$ | nr. | $f_{N,num}$ | $f_{N,exp}$ |
|---|---|---|---|---|---|---|---|---|
| 1. | 39.024 | 70.481(1) | 14. | 913.16 | 996.4 (20) | 26. | 1488.5 | 1325.9 (30) |
| 2. | 189.99 | 159.73 (2) | 15. | 918.48 | 935.33(19) | 27. | 1531.6 | – |
| 3. | 206.94 | 214.06 (4) | 16. | 936.59 | – | 28. | 1586.5 | 1540.0 (34) |
| 4. | 272.71 | 397.12 (7) | 17. | 982.85 | 1053.1 (21) | 29. | 1661.5 | – |
| 5. | 351.91 | – | 18. | 991.05 | 1094.9 (23) | 30. | 1790.6 | – |
| 6. | 417.18 | – | 19. | 1112.8 | – | 31. | 1792.0 | – |
| 7. | 470.94 | – | 20. | 1203.6 | 1236.7 (28) | 32. | 1849.2 | 1762.9 (39) |
| 8. | 478.16 | 441.9 (8) | 21. | 1363.5 | 1399.7 (32) | 33. | 1854.9 | – |
| 9. | 493.92 | 523.23 (10) | 22. | 1380.2 | – | 34. | 1876.1 | 1730.0 (38) |
| 10. | 573.54 | 625.84 (12) | 23. | 1416.3 | – | 35. | 1887.0 | – |
| 11. | 651.07 | 701.35 (13) | 24. | 1450.4 | – | 36. | 1900.1 | – |
| 12. | 686.97 | – | 25. | 1470.9 | – | 37. | 1998.8 | – |
| 13. | 737.57 | 814.12 (16) | | | | 38. | 2072.4 | 1907.8 (41) |

rubber strings and the shaker will add stiffness, mass or damping to the structure, hence change the dynamic properties of the system.

Secondly, the orientation of the layers may not be perfect. This hypothesis is supported by the observation that the numerical frequencies are lower than the experimental modes, except the second and eighth mode. These are the first and second bending mode over the width of the skin–stiffener, indicating deviating material properties in that direction; The combination observed of over– and underestimation is likely to be caused by non-perfect fibre orientation in the layers. A misalignment of the fibres causing a stiffness decrease in the $x$–direction inherently causes a stiffness increase in the $z$–direction and higher natural frequencies – as observed. Moreover, the a–symmetry in the mode shapes measured also suggests deviations in the fibre orientation.

Thirdly, the material properties can be slightly different. The material properties used in the numerical model (see table 1) apply to the slender beam with single stiffener, which is a different batch than the material from which the skin–stiffener structure was manufactured.

Finally, the modal density is relatively high, which complicates the experimental identification of mode shapes as they interfere with each other. As a consequence, the match between an experimental mode and a numerical mode can be poor. Moreover, the excitation point is for some modes close to a point with a low amplitude, resulting in a low response of that mode.

The first modes found in the measurements and the first modes calculated by the numerical model are shown in figure 7. The main conclusion that can be drawn from this comparison is that a model update is required. As mentioned, the results of the experiments and numerical model of the slender strip with single stiffener agreed quite well. Therefore the model improvements must be sought in the items mentioned above.

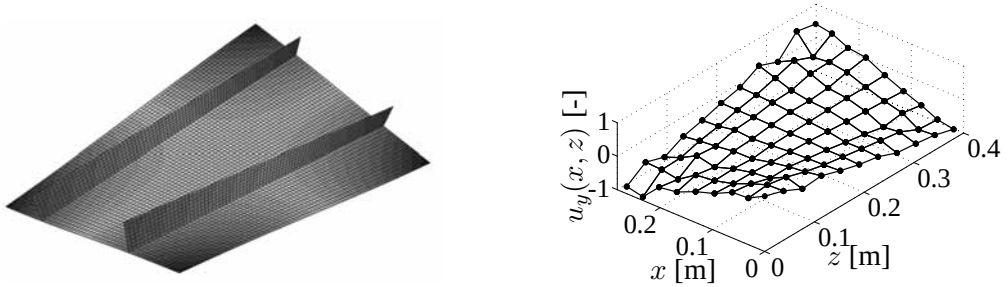


(a) *Mode 1 - numerical (left)* $F_N = 39.024$ *Hz and experimental (right)* $F_N = 70.481$ *Hz.*

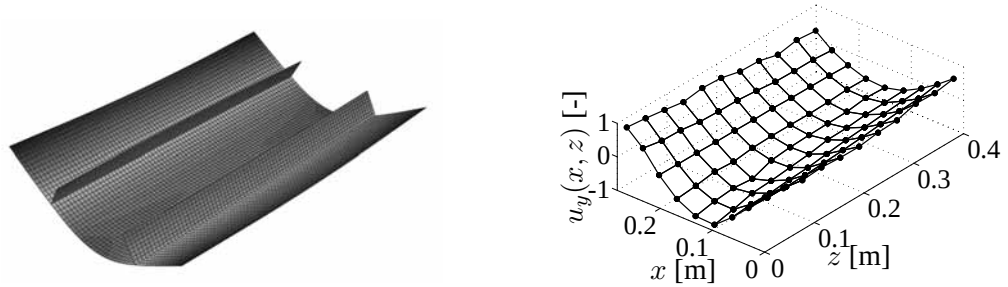


(b) *Mode 2 - numerical (left)* $F_N = 189.99$ *Hz and experimental (right)* $F_N = 159.73$ *Hz.*

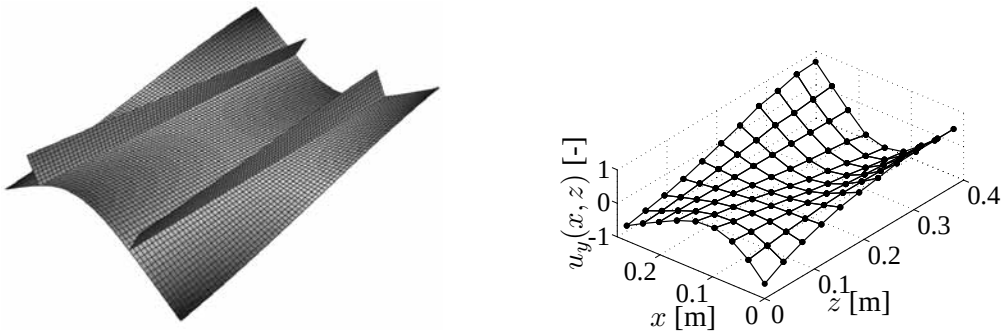


(c) *Mode 3 - numerical (left)* $F_N = 206.94$ *Hz and experimental (right)* $F_N = 214.06$ *Hz.*

Figure 7: *First three modes numerical (left) and experimental (right) (only skin visualised). The displacements* $u_y(x, z)$ *are normalised to a maximum absolute amplitude equal to unity.*

## 6.2 Comparison with measured damage index

The purpose of using a numerical analysis is to support the prediction of the location and the size of the damage based on experimental results. Therefore, the experimentally determined damage index [6] is compared

to the numerical results. Due to the limited comparison between the mode shapes (see table 4), a limited set of mode shapes is considered in the analysis (figure 8(a): full set, (b) limited set). Only those mode shapes with strong correlation between the experimental mode shape and the numerical mode shape are taken into account. The list consists of numerical modes 1, 2, 3, 8, 13, 15, 20, 26, 28 and 38 and their experimental counterpart.

Visual inspection of the skin–stiffener structure lead to the conclusion that a delamination is found between the first plies on the side of the stiffeners, with its centre approximately in $(x, z) \approx (-0.071, 0.115)$m. The impact load was applied on the opposing face of the skin, at approximately $(x, z)_{\text{impact}} \approx (-0.071, 0.200)$m. The delamination appears to be oriented in the -45° direction, corresponding to the direction of the fibres in the top ply. The length of the visible damage is approximately 0.035m, whereas the maximum width equals approximately 0.015m. Assuming an elliptically shaped delamination, this corresponds to the case $R_1 = 0.015$m, $R_2 = 0.035$m and $\theta = -45^{\circ}$. The results of this case are shown in figure 8(c) and (d). Noted that the exact size of the delamination is still unknown.

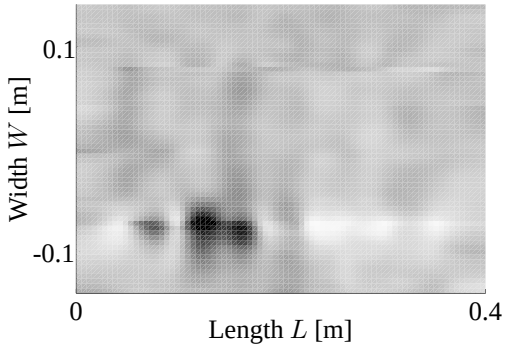


(a) *Damage index $\beta$ based on the full set of experimentally determined mode shapes [6]. $\beta_{max} = 4.94$. Grey scale limit: [0,4].*

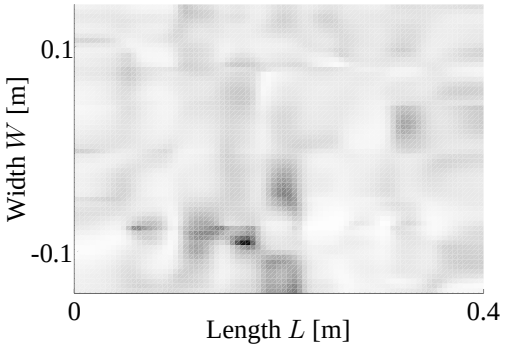


(b) *Damage index $\beta$ based on a limited set of experimentally determined mode shapes [6]. $\beta_{max} = 9.43$. Grey scale limit: [0,10].*

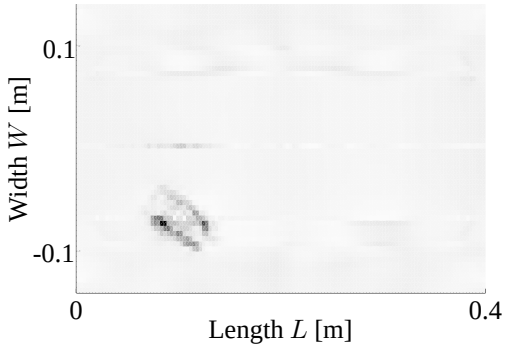


(c) *Damage index for an elliptically shaped delamination with radii $R_1 = 0.015$m and $R_2 = 0.035$m, which centre is located at $(x_e, z_e) = (-0.071, 0.1)$m, oriented at $\theta_{xz} = -45^{\circ}$. $\beta_{max} = 24.88$. Grey scale limit: [0,20].*

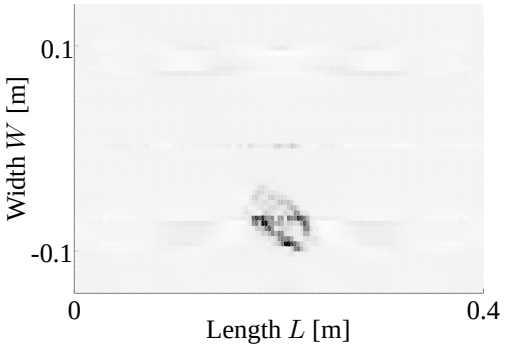


(d) *Damage index for an elliptically shaped delamination with radii $R_1 = 0.015$m and $R_2 = 0.035$m, which centre is located at $(x_e, z_e) = (-0.071, 0.2)$m, oriented at $\theta_{xz} = -45^{\circ}$. $\beta_{max} = 29.44$. Grey scale limit: [0,20].*

Figure 8: *Comparison between the experimentally and numerically determined damage index. The darker colour corresponds to a higher damage index.*

There are significant differences between the figures. The limited set, figure 8(b), appears to contain an insufficient number of modes to predict the damage accurately. The numerically calculated damage indices shown very little correspondence to the measured damage indices. This can for a large part be explained by a two reasons.

1. It is not unlikely that other plies than the top ply are damaged or that the thermoplastic filler is separated

from the skin over a certain length. A C–scan can be used to determine the exact dimensions and location and is scheduled as future work.

2. The number of data points is substantially higher in the numerical model (9×11 versus 57×81), leading to a higher value of the damage index. As a result it provides more information in the neighbourhood of the stiffener (see figure 9). This topic will be addressed in the section 6.3.

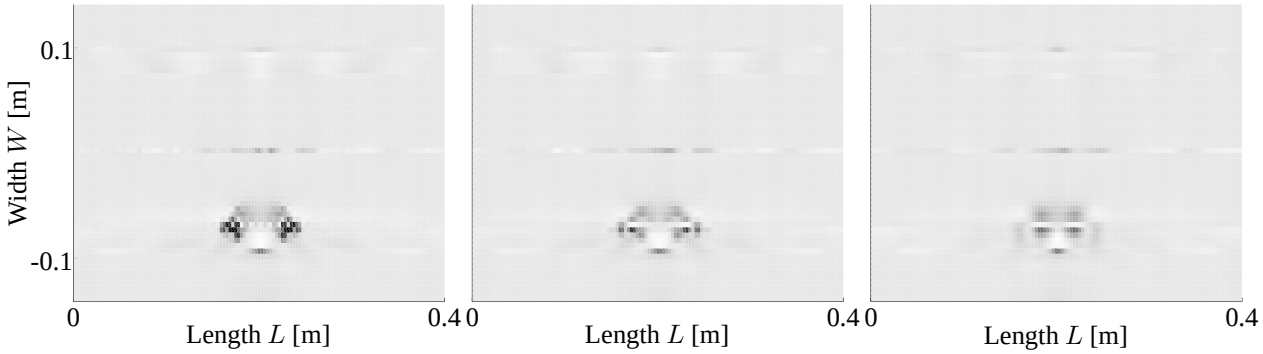


(a) *81 points,* $\beta_{max} = 13.8$. (b) *41 points,* $\beta_{max} = 8.16$. (c) *21 points,* $\beta_{max} = 5.99$.

Figure 9: *Effect of the number of evaluation points on the maximum level and smoothness of the damage index* $\beta$ *for an elliptically shaped delamination with radii* $R_1 = 0.015$*m and* $R_2 = 0.035$*m, which centre is located at* $(x_e, z_e) = (-0.071, 0.2)$*m and oriented at* $\theta_{xz} = 0^{\circ}$*. The darker colour corresponds to a higher damage index, a grey scale range of [0,10] is used for all graphs.*

There are also two other differences between the numerical model and the measurements. These differences are expected to be of minor influence on the damage index.

1. No contact is defined between the surfaces in the delamination. A higher damage index is expected for the numerical model compared to the experimental values due the absence of contact (compare the free and constraint mode model of Della and Shu [30].

2. The delamination is located halfway the thickness rather than at the top. However, the effect of the location in thickness direction of the delamination on the bending stiffness is minor, hence will be its effect on the damage index. Moreover, the actual delamination is likely to extent to multiple layers, which is not modelled.

## 6.3 Damage index for various cases

The damage index $\beta$ (10) is calculated for the cases listed in table 3. The index can be calculated based on the displacements along lines parallel to the $x$–axis ($u_y(x)$) and along lines parallel to the $z$–axis ($u_y(z)$). It was observed during analysis of the experimental results [6] that the latter approach provides significantly more sensitive results. A delamination close to the stiffener results in a relatively high loss of stiffness in the direction the stiffener. This is confirmed by the numerical results, as can be seen in figure 10. In other words, the sensitivity of the damage index $\beta$ of structures with an anisotropic stiffness distribution is reduced in the direction of the lower stiffness, complicating the detection of damage.

The orientation of the delamination is clearly visible in the damage index plots based on the numerical model, as can be observed in figure 11. However, the largest peaks are found close to the stiffener. As a result it may be difficult to distinguish between a relatively slender delamination ($R_1 \ll R_2$) oriented at 45° and a relatively round delamination ($R_1 \approx R_2$) oriented at for example 0°. The dots in figure 11 indicate the location where the response was measured in the experiments [3]. The spline functions, used to be able to calculate the mode shapes and its derivatives, is fit based on these points only. Adding that there generally is

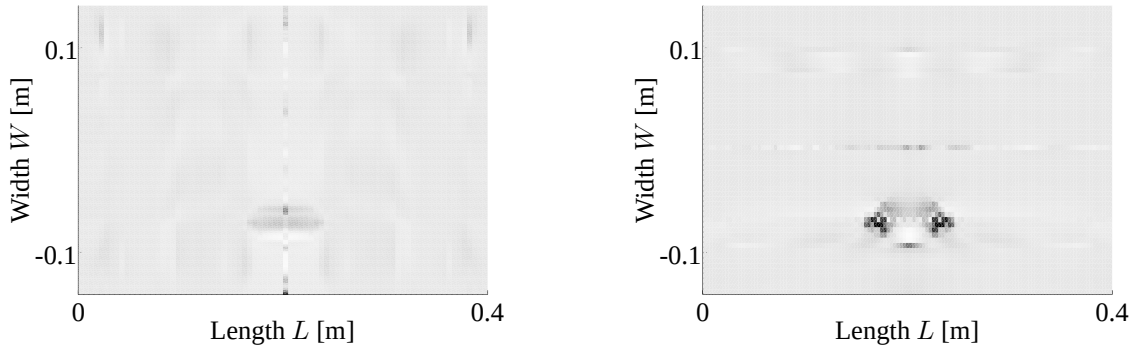


(a) *Damage index $\beta$ based on $u_y(x)$. $\beta_{max} = 7.85$*

(b) *Damage index $\beta$ based on $u_y(z)$. $\beta_{max} = 13.8$*

Figure 10: *Damage index for an elliptically shaped delamination with radii $R_1 = 0.015$m and $R_2 = 0.035$m, which centre is located at $(x_e, z_e) = (-0.071, 0.2)$m and oriented at $\theta_{xz} = 0^{\circ}$. The darker colour corresponds to a higher damage index. The grey scale range is set to [0,10].*

a certain amount of noise present in the measurement, it is likely that the orientation of the damage will not be captured. The damage index based on $u_y(x)$ is not sufficiently sensitive to support the distinction between delaminations with different orientations.

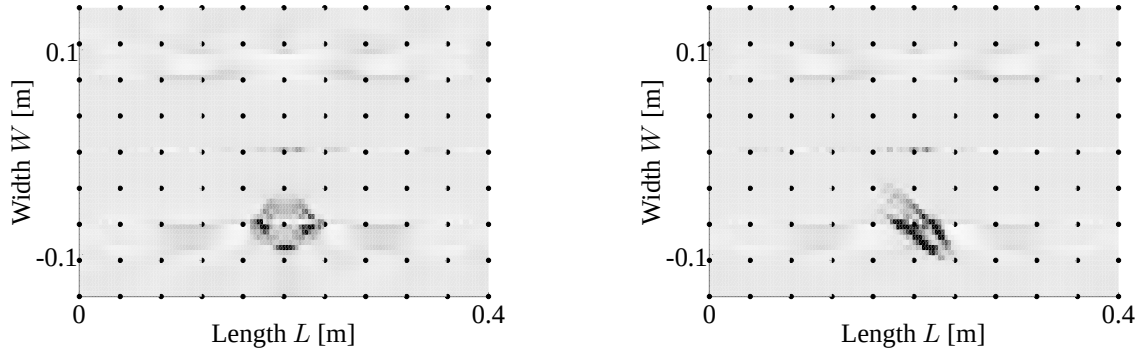


(a) *Damage index $\beta$ based on $u_y(z)$, $R_1 = 0.02$m, $R_2 = 0.025$m, $\theta = 0^{\circ}$.*

(b) *Damage index $\beta$ based on $u_y(z)$, $R_1 = 0.01$m, $R_2 = 0.045$m, $\theta = 45^{\circ}$.*

Figure 11: *Comparison of slender versus round delamination. The centre of both delaminations is located at $(x_e, z_e) = (-0.071, 0.2)$m. The darker colour corresponds to a higher damage index, the dots to the locations where the response was measured in the experiments [6].*

# 7 Conclusions & future outlook

The first results of a numerical model of a skin-stiffener structure with a delamination were compared to experimental results on a composite skin–stiffener structure with an impact induced damage. A number of conclusions can be drawn.

The numerical model must be adapted in order to find a better match with the experimental results. This does not only concern the implementation of the material model, but also the implementation of the delamination.

However, the numerical model does provide some useful information on the effect of a delamination on the damage index. The first observation is that anisotropy in the stiffness distribution affects the damage index negatively in the direction of the lowest stiffness. It will therefore also be difficult to detect the orientation of a delamination accurately with the current experimental set–up. The location of the delamination along the direction of highest stiffness is of limited influence on the result.

Future work involves in the first place C–scan measurements to reveal the actual size and location of the damage. Secondly, the numerical models will be improved to obtain a better match with the experimental results. The material properties and/or model will be adapted as required. Moreover, contact will be included and a transient analysis will be performed to assess the influence of non–linearities.

## References

[1] W.J.B. Grouve, L. Warnet, A. de Boer, R. Akkerman, and J. Vlekken. Delamination detection with fibre bragg gratings based on dynamic behaviour. *Composites Science and Technology*, 68(12):2418–2424, 2008.

[2] N. Stubbs, J.T. Kim, and C.R. Farrar. Field verification of a nondestructive damage localization and severity estimation algorithm. In *Proceedings of the 13th International Modal Analysis Conference*, pages 210–218, 1995.

[3] T.H. Ooijevaar, R. Loendersloot, L.L. Warnet, A. de Boer, and R. Akkerman. Vibration based structural health monitoring of a composite t–beam. *Composite Structures*, 92(9):2007–2015, 2009.

[4] R. Loendersloot, T.H. Ooijevaar, L. Warnet, R. Akkerman, and A. de Boer. Vibration based structural health monitoring in fibre reinforced composites employing the modal strain energy method. In J.F.S. Gomes and S.A. Meguid, editors, *Proceedings of the International Conference Integrity Failure and Reliability - 3*, page 16p, 2009.

[5] R. Loendersloot, T.H. Ooijevaar, L. Warnet, R. Akkerman, and A. de Boer. *Vibration and Structural Acoustics Analysis*, chapter Vibration based structural health monitoring in fibre reinforced composites employing the modal strain energy method., page 31p. Springer, 2010. accepted for publication.

[6] T.H. Ooijevaar, L.L Warnet, R. Loendersloot, and A. de Boer. Vibration based structural health monitoring of a composite plate structure with multiple stiffeners. In *Proceedings of the European Workshop on Structural Health Monitoring*, 2010. accepted.

[7] J.-T. Kim and N. Stubbs. Model uncertainity impact and damage-detection accuracy in plate grider. *Journal of Structural Engineering*, 121(10):1409–1417, 1995.

[8] C.R. Farrar and D.A. Jauregui. Comparative study of damage identification algorithms applied to a bridge: I experiment. *Smart Materials and Structures*, 7(5):704–719, 1998.

[9] C.R. Farrar and D.A. Jauregui. Comparative study of damage identification algorithms applied to a bridge: II numerical study. *Smart Materials and Structures*, 7(5):720–731, 1998.

[10] J.-T. Kim and N. Stubbs. Improved damage identification method based on modal information. *Journal of Sound and Vibration*, 252(2):223–238, 2002.

[11] A.K. Pandey, M. Biswas, and M.M. Samman. Damage detection from changes in curvature mode shapes. *Journal of Sound and Vibration*, 145(2):321–332, 1991.

[12] A.K. Pandey and M. Biswas. Damage detection in structures using changes in flexibility. *Journal of Sound and Vibration*, 169(1):3–17, 1994.

[13] D.C. Zimmerman and M. Kaouk. Structural damage detection using a minimum rank update theory. *Journal of Vibration and Acoustics*, 116(2):222–231, 1994.

[14] T. Toksoy and A.E. Aktan. Bridge-condition assessment by modal flexibility. *Experimental Mechanics*, 34(3):271–278, 1994.

[15] A.A. Alvandi and C.B. Cremona. Assessment of vibration-based damage identification techniques. *Journal of Sound and Vibration*, 292(1-2):179–202, 2006.

[16] H. Li, H. Fang, and S.-L.J. Hu. Damage localization and severity estimate for three-dimensional frame structures. *Journal of Sound and Vibration*, 301:481–494, 2007.

[17] H. Li, H. Yang, and S.-L.J.B Hu. Modal strain energy decomposition method for damage localization in 3d. *Journal of Engineering Mechanics*, 132(9):941–951, 2006.

[18] M. Kumar, R.A. Shenoi, and S.J. Cox. Experimental validation of modal strain energies based damage identification method for a composite sandwich beam. *Composites Science and Technology*, 69:1635–1643, 2009.

[19] P. Cornwell, S.W. Doebling, and C.R. Farrar. Application of the strain energy damage detection method to plate-like structures. *Journal of Sound and Vibration*, 224(2):359–374, 1999.

[20] S. Choi, S. Park, and N. Stubbs. Nondestructive damage detection in structures using changes in compliance. *International Journal of Solids and Structures*, 42:4494, 4513 2005.

[21] S. Choi, S. Park, N.-H. Park, and N. Stubbs. Improved fault quantifcation for a plate structure. *Journal of Sound and Vibration*, 297:865–879, 2006.

[22] B.H. Kim, N. Stubbs, and T. Park. Flexural damage index equations of a plate. *Journal of Sound and Vibration*, 283:341–368, 2005.

[23] J.B. Schwarz and M.H. Richardson. *Experimental modal analysis*. Vibrant Technology Inc., 1999.

[24] S. Choi and N. Stubbs. Damage identification in structures using the time-domain response. *Journal of Sound and Vibration*, 275:557–590, 2004.

[25] B.H. Kim, N. Stubbs, and T. Park. A new method to extract modal parameters using output-only responses. *Journal of Sound and Vibration*, 282:215–230, 2005.

[26] A. Offringa, J. List, J. Teunissen, and H. Wiersma. Fiber reinforced thermoplastic butt joint development. In *Proceedings of International SAMPE Symposium and Exhibition*, 2008. 16 pages.

[27] T.A. Duffey, S.W. Doebling, C.R. Farrar, W.E. Baker, and W.H. Rhee. Vibration-based damage identification in structures exhibiting axial and torsional response. *Journal of Vibration and Acoustics*, 123(1):84–91, 2001.

[28] R. de Vries, E.A.D. Lamers, S. Wijskamp, B.H. Villa Rodriguez, and R. Akkerman. The university of twente micromechanics modeller. Technical report, University of Twente, 2004. www.pt.ctw.utwente.nl/organisation/tools/.

[29] I. Ullah and J.K. Sinha. Dynamic study of a composite plate with delamination. In *Proceedings of the Third International Conference on Integrity, Reliability and Failure*, 2009. 15 pages, S1145 P0506.

[30] C.N. Della and D. Shu. Vibration of delaminated composite laminates: A review. *Applied Mechanics Reviews*, 60(1-6):1–20, 2007.